*Korean J. Chem. Eng.*, 39(9), 2482-2490 (2022)
DOI: 10.1007/s11814-022-1176-2

pISSN: 0256-1115
eISSN: 1975-7220

# Ion-imprinted antifouling nanocomposite membrane for separation of lithium ion

**Dongshu Sun*,**,***, Tianyu Zhou*,**,***, Yang Lu****, Yongsheng Yan*, Chunbo Liu*,**,***,†, and Guangbo Che*,*****,†**

*Key Laboratory of Preparation and Applications of Environmental Friendly Materials (Jilin Normal University), Ministry of Education, Changchun, 130103, China
**Key Laboratory of Environmental Materials and Pollution Control, the Education Department of Jilin Province, Jilin Normal University, Siping, 136000, China
***College of Environmental Science and Engineering, Jilin Normal University, Siping, 136000, China
****Jilin Provincial Key Laboratory for Numerical Simulation, Jilin Normal University, 1301 Haifeng Street, Siping, 136000, China
*****School of Chemistry, Baicheng Normal University, Baicheng 137099, P. R. China
(*Received 13 October 2021 • Revised 7 May 2022 • Accepted 11 May 2022*)

**Abstract**−Membrane fouling is a primary challenge restricting the practical application of membrane separation technology. Inspired by the idea that improving hydrophilicity would lead to antifouling performance of membrane material. In this work, ion-imprinted antifouling nanocomposite membrane (LiI-NcMs) blended with GO and $TiO_2$ nanomaterial was fabricated for selective separation of lithium ion. As a result, markedly improved hydrophilicity was achieved on LiI-NcMs (55.1° for contact angle). LiI-NcMs also showed good selective adsorption capacity in the mixed solution of $Mg^{2+}$ and $Li^+$. Moreover, LiI-NcMs exhibited superior stability; after 20 adsorption/desorption cycles a maximum adsorption capacity of 88.1% can be maintained. This work demonstrates a new and facile approach to prepare novel membrane separation material for a particular substance for efficient selective separation in industrial applications.

Keywords: Antifouling, Hydrophilicity, Imprinted, Membranes, Lithium Ion

## INTRODUCTION

With the sustained and rapid development of electronic industry, especially electric cars, the lithium ion battery has become the mainstream battery. Therefore, making the best of lithium resources remains significantly important for economic development [1-3]. According to the statistics, about 70 percent of lithium resources are found in seawater and salt lakes. Thus, establishing a green and efficient method for enrichment and separation of lithium ion from water environment is highly necessary.

Membrane separation technology is deemed to be a desired alternative due to its high porosity, large surface area, and cost effectiveness [4-6]. Polytetrafluoroethylene (PVDF) is usually used as membrane substrate material on account of low cost, high mechanical strength and good thermal stability. However, the applications are always restricted; one side is the lack of specific selectivity. To get selective separation, molecular (ion) imprinting technique creates specific recognition sites using template molecules (ion), which has been usually applied to membranes to obtain molecularly (ion) imprinted membranes. More recently, molecularly (ion) imprinted membranes have attracted intensive interest of both academic and industries [7-10].

However, antifouling performance of the membrane-based treatment has also restricted its application, which reduces the service life of membrane separation materials [11-14]. Generally, the main reason for membrane fouling is the hydrophobic property of PVDF material, which usually leads to organic colloid pollutants accumulated on the membrane surface [15,16]. Thus, it is necessary to improve the antifouling performance of PVDF material.

Some progress has been recently achieved to improve the antifouling performance of membrane material, such as grafting hydrophilic groups, coating or blending nanomaterials [17-19]. Over the past decades, graphene oxide (GO) has spurred interest in designing novel graphene-based materials for its two-dimensional construction and easy functionalization [20,21]. More importantly, GO-based membrane will form nanochannels by GO sheets, which is desired for better separation performance of membrane separation materials for ions [22].

However, the GO-based membrane bound via $\pi$-$\pi$ interactions and hydrogen bonding gives poor strength to the sheets [22]. Titanium dioxide ($TiO_2$) is applied most widely in the fields of modification membranes and pollutant degradation due to superior effectiveness, cheapness, and chemical stability [23,24]. In this study, GO and $TiO_2$ were selected as the targeted materials to improve the hydrophilicity and strength of the membrane material. We prepared a novel imprinted composite membrane modified with GO and $TiO_2$ composite nanomaterials; the antifouling performance and hydrophily were explored by BSA adsorption experiment and water contact angle test. Selectivity and potential applications were investigated in detail based on selective rebinding and static permeation. The as-obtained composite membranes achieved excellent selective recognition ability and anti-pollution ability. Meanwhile, novelty

†To whom correspondence should be addressed.
E-mail: guangboche@jlnu.edu.cn

product would play a positive role in promoting the development and applications of membranes in selectively separating $Li^+$ in water.

## EXPERIMENTAL

### 1. Materials

Polyvinylidene fluoride (PVDF) was purchased from Arkema, France. Polyvinylpyrrolidone (PVP-K30), grapheme powder, bovineserum albumin (BSA, Mn=68,000), tetra-n-butyl titanate (TNBT), glacial acetic acid and methylene blue (MB) were purchased from Aladdin Reagent. N,N-dimethylacetamide (DMAC), N,N-dimethylformamide (DMF), N,N-dimethylethylenediamine (DMDA), 2-methylol-12-crown-4 (2M12C4), 3-methacryloxypropyltrimethoxysilane (MPTS), ethylene glycol dimethacrylate (EGDMA), olefin Propyl bromide, hydroquinone, sodium carbonate ($Na_2CO_3$), sodium hydroxide (NaOH), azobisisobutyronitrile (AIBN) lithium chloride (LiCl), sodium chloride (NaCl), potassium chloride (KCl ), Magnesium chloride ($MgCl_2$), calcium chloride ($CaCl_2$), barium chloride ($BaCl_2$), hydrogen peroxide (30%) and methanol were purchased from Sinopharm Group Chemical Reagent. Sodium nitrate ($NaNO_3$), potassium permanganate ($KMnO_4$), hydrochloric acid (HCl) and sulfuric acid ($H_2SO_4$) were purchased from Beijing Chemical Works. The experimental water is double distilled water.

### 2. Methods

2-1. Fabrication of Composite Nanomaterial

Graphene oxide (GO) was synthesized from graphite powder (Kropfmühl AG, Germany) according to the modified Hummers method [25].

Drops of 10 mL tetra-n-butyl titanate were added to 30 mL ethanol under stirring for 10 min to form a light yellow clear solution A. The other side, drops of 4 mL glacial acetic acid and 10 mL deionized water wer added to 35 mL ethanol under stirring for 30 min at pH≤3 to form solution B. Then, solution A was added to solution B to obtain la ight yellow solution, stirred in 40 °C thermostatic water bath. After 2 h, the solution turned to white gel, and then yellow crystals were obtained under vacuum drying at 60 °C. Calcination at 500 °C was carried out for 2 h in an argon atmosphere to obtain highly crystalline $TiO_2$ power.

0.06 g GO was dispersed in 60 mL deionized water and 30 mL ethanol by sonication for 30 min, 0.6 g $TiO_2$ was added into above solution under vigorous stirring for 2 h, then autoclaved in a Teflon-lined stainless steel vessel at 120 °C for 3 h. After the hydrothermal reaction, the mixture was centrifuged and washed with deionized water to remove organic components and obtain highly crystalline GR/$TiO_2$ composite nanomaterial after vacuum drying at 60 °C. Under such a solvothermal condition, the solvent of ethanol-water has strong power to reduce GO to GR [26].

2-2. Preparation of Li-imprinted Nanocomposite Membranes (LiI-NcMs)

The nanocomposite membranes were prepared by phase inversion process. 0.1 g GR/$TiO_2$, 4 g PVDF powder, 25 mL DMAc and 0.1 g PVP were mixed into a three-necked round-bottomed flask; the mixture was mechanically stirred (400 rpm) for 24 h at 25 °C. The obtained casting solution was let stand for 24 h to eliminate bubbles. Next, the casting solution was poured on a film applicator to set the film thickness, and then the glass plate was immersed in deionized water. After the phase inversion process, the obtained nanocomposite membranes were stored in deionized water.

The above-prepared nanocomposite membranes were first modified with MPTS, and polymerizable double bond was introduced for further blotting. The nanocomposite membranes and 2 mL MPTS were added to 60 mL ethanol/water (4 : 1, v : v) mixed solution and magnetically stirred (80 rpm) for 24 h at 80 °C. The resulting membranes were rinsed with deionized water and ethanol for three times each.

The functional monomer of 2AM12C4 was synthesized according to our previous work [27]. 5 mmol 2AM12C4 and 5 mmol LiCl were added to 60 mL of methanol and stirred at 25 °C for 2 h. Then 25 mmol MAA, 0.1 mol EGDMA, 0.05 g AIBN and above-prepared membranes were added to the above mixture and refluxed at 60 °C under nitrogen atmosphere overnight. Finally, the resulting membranes were eluted with 0.5 mol $L^{-1}$ HCl to remove $Li^+$ and rinsed with deionized water and ethanol, and then dried at 50 °C in a vacuum overnight, which indicates the LiI-NcMs. The synthesis process of NI-NcMs is similar to that of LiI-NcMs, except that $Li^+$ was not added during the synthesis.

### 3. Characterization

Microstructures on sponges were observed by scanning electron microscope (SEM, JSM-7001F, Japan). Surface morphologies were characterized by transmission electron microscope (TEM, Tecnai 12, Holland). The crystal structure was detected by X-ray diffraction (XRD, D/max 2500/PC, Japan). The hydrophilicity of membranes was investigated by observing water contact angles based on contact angle measuring instrument (CAMI, KSV CM200, Finland). The lithium ion concentration was determined by using inductively coupled plasmatomic emission spectroscopy (ICP, VISTA-MPX, Australia).

### 4. Antifouling Performance Experiments

BSA was used as a template protein to study static and dynamic protein adsorption experiments to evaluate the antifouling performance of the prepared membranes. The prepared membranes were immersed in Tris-HCl aqueous solution (0.1 M, pH=7.4) for 5 min and then added into 50 mL of BSA aqueous solution (1.0 mg $mL^{-1}$, pH=7.4), sealed and adsorbed for 24 h at room temperature. The adsorption capacity of above-prepared membranes for BSA was obtained by measuring the concentration of BSA solution. At the same time, each dynamic adsorption experiment was conducted during the shaking process under simulated real conditions. Concentration of BSA was determined by UV-Vis spectrophotometer.

### 5. Performance of Membranes

5-1. Static Adsorption Experiments

In the isothermal adsorption study, one piece of LiI-NcMs or NI-NcMs was immersed in the $Li^+$ aqueous solution with different initial concentrations (2, 5, 8, 10, 15, 20, 30, 50 mg/L). The concentration of $Li^+$ by ICP was determined at the moment the adsorption reached equilibrium. The equilibrium adsorption capacity of LiI-NcMs and NI-NcMs was calculated by the following:

$$Q_e = \frac{(C_0 - C_e)V}{m} \quad (1)$$

$Q_e$ (mg $g^{-1}$) is the equilibrium adsorption capacity of LiI-NcMs and NI-NcMs, $C_0$ (mg $L^{-1}$) and $C_e$ (mg $L^{-1}$) are the initial and equilib-

rium concentrations of $Li^+$, respectively. V (L) is the volume of the solution and m (g) is the mass of LiI-NcMs and NI-NcMs.

Kinetic adsorption studies were performed by immersing one piece of LiI-NcMs or NI-NcMs in $Li^+$ aqueous solution (10 mg $L^{-1}$). At different time intervals (5, 10, 20, 30, 60, 100, 120, 180 min), the adsorbed solution was then taken out to determine the concentration of $Li^+$. The adsorption amount of adsorption of LiI-NcMs and NI-NcMs was calculated at different times according to Eq. (2):

$$Q_t = \frac{(C_0 - C_t)V}{m} \quad (2)$$

$Q_t$ (mg $g^{-1}$) is the adsorption amount of LiI-NcMs and NI-NcMs at different time t, $C_0$ (mg $L^{-1}$) and $C_t$ (mg $L^{-1}$) are the initial concentrations and the concentrations at time t of $Li^+$. V (L) is the volume of the solution and m (g) is the mass of LiI-NcMs and NI-NcMs.

5-2. Membrane Flux Experiments

The LiI-NcMs and PVDF membranes were fixed on a membrane flux testing device; the effective area of test membranes was 4.8 $cm^2$ under 0.15 Mpa. The concentration of LiCl aqueous solution was 20 mg/L. At different time intervals, the solution was taken out to determine the volume of the solution. The membrane flux of LiI-NcMs and PVDF membrane was calculated from Eq. (3):

$$J_m = \frac{V}{St} \quad (3)$$

where, $J_m$ (mL $cm^{-2}$ $min^{-1}$) and V (mL) represent the membrane flux and volume of the solution after penetration, t (min) and s ($cm^2$) represent the sampling time and effective area of the test membranes.

5-3. Selective Adsorption Experiments

In selective adsorption experiments, $Mg^{2+}$ was selected as the competitive ion, which is the most representative and difficult component to separate. The LiI-NcMs was immersed in the mixture of $Li^+$ and $Mg^{2+}$. According to the actual conditions, the concentration of $Mg^{2+}$ was 200 mg/L and $Li^+$ was 2, 5, 8, 10, 15, 20, 30 and 50 mg $L^{-1}$, respectively. After adsorption reached equilibrium, the concentration of $Li^+$ and $Mg^{2+}$ was determined by ICP. The adsorption capacity of LiI-NcMs and NI-NcMs was calculated by Eq. (1).

5-4. Selective Permeation Experiments

The permselectivity of LiI-NcMs or NI-NcMs was tested by competitive penetration experiments. The test was in an H-type device with an effective membrane contact area of 1.5 $cm^2$. 100 mL of a mixed aqueous solution of $Li^+$, $K^+$, $Na^+$ and $Mg^{2+}$ was placed as feed solution in the left chamber, and 100 mL of deionized water was placed as receiving solution in the right chamber. The device was placed in a constant temperature water bath shaker to keep the solution uniform. At different time points (5, 15, 30, 45, 60, 120, 180 min), 5 mL receiving solution was taken to determine the ion concentration, and then 5 mL deionized water was added to the receiving phase. The final data is the average of three sets of parallel tests. Permeation flux $J_x$ (mg $cm^{-1}$ $h^{-1}$), permeability coefficient P ($cm^2$ $h^{-1}$) and selective permeability factor $\beta$ were calculated by the following:

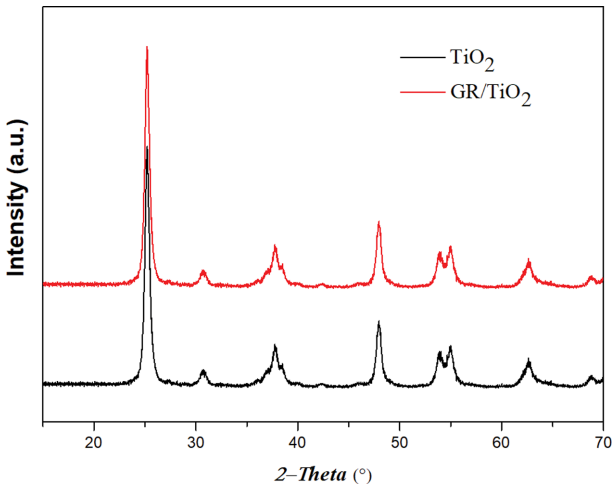


**Fig. 1. XRD patterns of $TiO_2$ and GR/$TiO_2$.**

$$J_x = \frac{\Delta C_x V}{\Delta t A} \quad x=Li^+, K^+, Na^+ \text{ and } Mg^{2+} \quad (4)$$

$$P = \frac{J_x d}{(C_{F_x} - C_{R_x})} \quad x=Li^+, K^+, Na^+ \text{ and } Mg^{2+} \quad (5)$$

$$\beta_{x/Li^+} = \frac{P_x}{P_{Li^+}} \quad x=K^+, Na^+ \text{ and } Mg^{2+} \quad (6)$$

where V, A and d represent the volume of the feed and receiving solution (mL), the effective membrane area ($cm^2$) and the membrane thickness, respectively. $\Delta C_x/\Delta t$ is the change concentration of the receiving solution. $(C_{F_x} - C_{R_x})$ is the concentration difference between feed solution and receiving solution.

## RESULTS AND DISCUSSION

### 1. Characterization

As shown in Fig. 1, the XRD pattern of GR/$TiO_2$ closely parallels $TiO_2$. The peaks at 2$\theta$ values of 25.3°, 37.8°, 48.0°, 53.9°, 55.1°, 62.7°, 68.8° can be indexed to (101), (004), (200), (105), (211), (204), (116) crystal planes of anatase $TiO_2$. Moreover, no diffraction peaks of GR were detected in the GR/$TiO_2$ nanocomposites, which may be because the main characteristic peak of GR might be shielded by the main peak of anatase $TiO_2$ [28] .

Fig. 2 provides the TEM images of GO, $TiO_2$ and GR/$TiO_2$. It is clear that the two-dimensional structure of GO sheets with micrometers-long wrinkles was demonstrated. This is due to the presence of a large number of oxygen-containing groups on the surface of GO, which is dispersed in the solution to form a single layer of GO. The images of $TiO_2$ show evenly dispersed nanoparticles. In the GR/$TiO_2$ nanocomposite, the GR sheets are well decorated by the $TiO_2$ nanoparticles and the micrometers-long wrinkles of GR/$TiO_2$ are still retained after the hydrothermal treatment.

The surface morphology of prepared membranes was observed by SEM. As shown in Fig. 3(a), PVDF membrane exhibits a porous and smooth surface structure after the phase inversion process. However, some agglomeration exists on the surface of the PVDF membrane; the reason should be ascribed to the casting solution

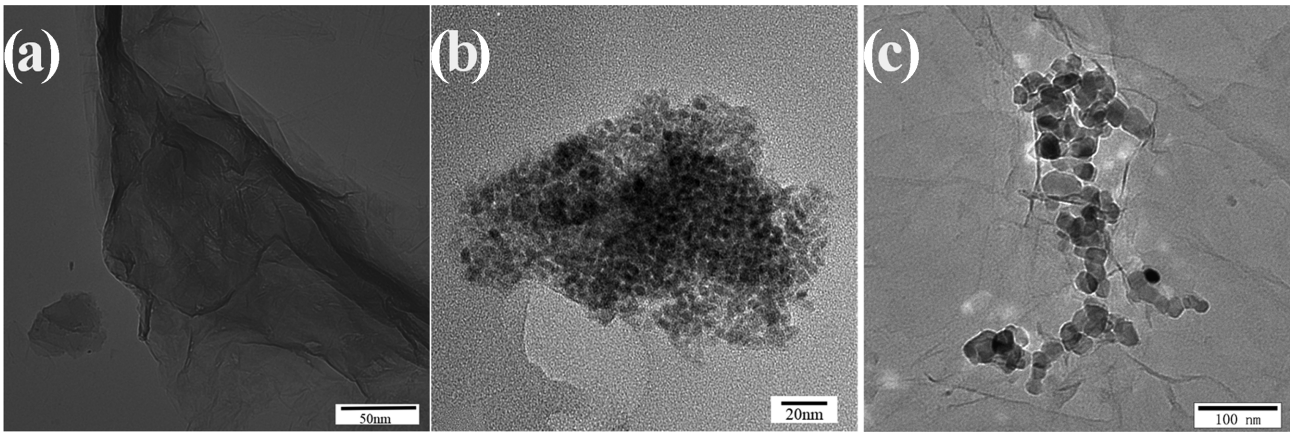


**Fig. 2. TEM images of (a) GO, (b) $TiO_2$ and (c) GR/$TiO_2$.**

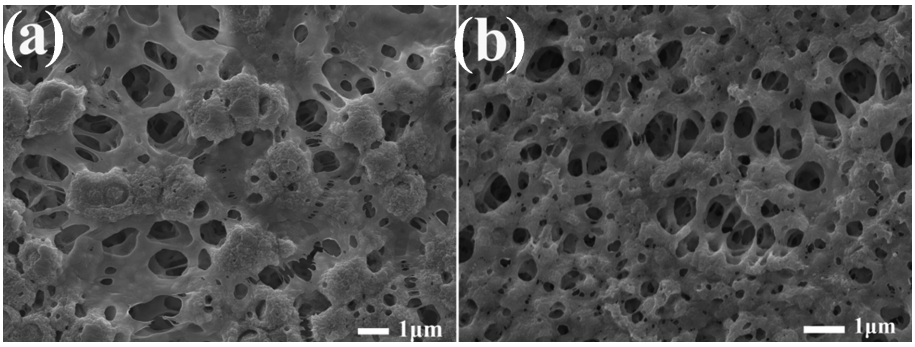


**Fig. 3. SEM images of (a) PVDF membrane and (b) LiI-NcMs.**

not being uniform and the speed of scraping was not constant. The smoother surface structure of PVDF membranes is to be expected. When the membrane was modified and imprinted, the obtained LiI-NcMs had a relatively rough surface morphology and significantly thicker polymer layer (Fig. 3(b)), indicating that a uniform imprinted layer had been successfully synthesized on the surface of the LiI-NcMs. Importantly, compared with PVDF membrane, the narrower pores of LiI-NcMs are achieved; the reason could be inferred that blending GO sheets formed two-dimensional grid construction, which is beneficial to interaction between $Li^+$ and $Li^+$-imprinted sites of LiI-NcMs.

**2. Analysis of Antifouling Performance**

To study the antifouling properties of the prepared membranes, static and dynamic BSA adsorption experiments were conducted. As shown in Fig. 4, the BSA adsorption capacity of LiI-NcMs and NI-NcMs shows lower than that of PVDF membrane, indicating that the antifouling property of modified membranes has been greatly improved. The reason should be attributed to blend GR/$TiO_2$ nanocomposite resulting in better antifouling property, which contributes to building a water film on the surface of membranes and restrains the contact between protein and membranes. This is undoubtedly beneficial for the enhancement of antifouling properties.

According to reports in the literature [16], the enhancement of the antifouling performance comes from the improved hydrophilicity of membranes. It is significantly necessary to investigate the hydrophilicity of the obtained membranes. As shown in Fig. 5(a),

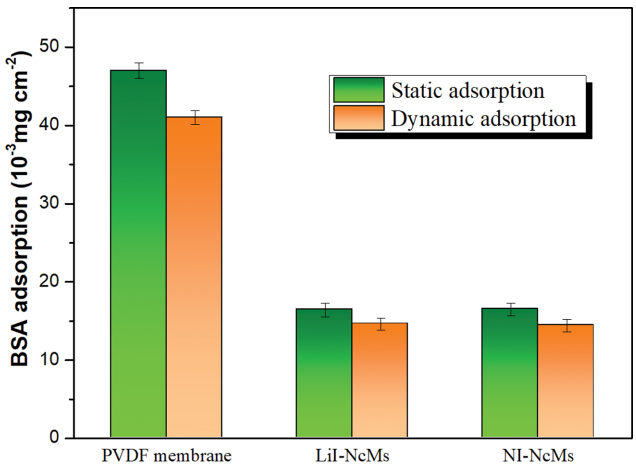


**Fig. 4. Adsorption capacity of BSA onto membranes. Error bars are standard deviations from three experiments with independently prepared membranes.**

the contact angle of PVDF membrane is 90.2° (hydrophobicity). In Fig. 5(b), the contact angle of GO/PVDF membrane is 63.4° (synthesized in our previous work [29]), demonstrating the effective improvement of the hydrophilicity by blending GO. It can be ascribed to that GO contains abundant oxygen-containing groups (hydroxyl, carboxyl, epoxide), which could effectively improve the hydrophilicity of the membranes. Expectantly, as shown in Fig. 5(c),

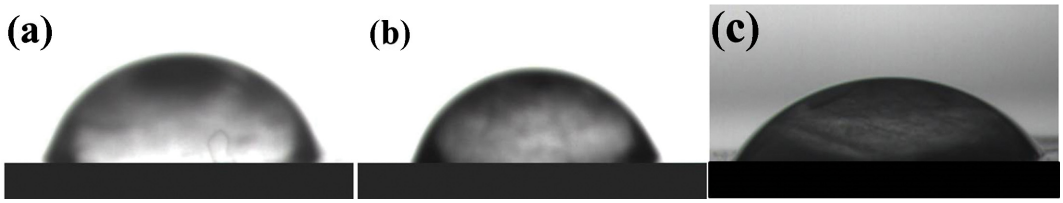


**Fig. 5. Water contact angle photographs of (a) PVDF membrane, (b) GO /PVDF membrane, (c) LiI-NcMs.**

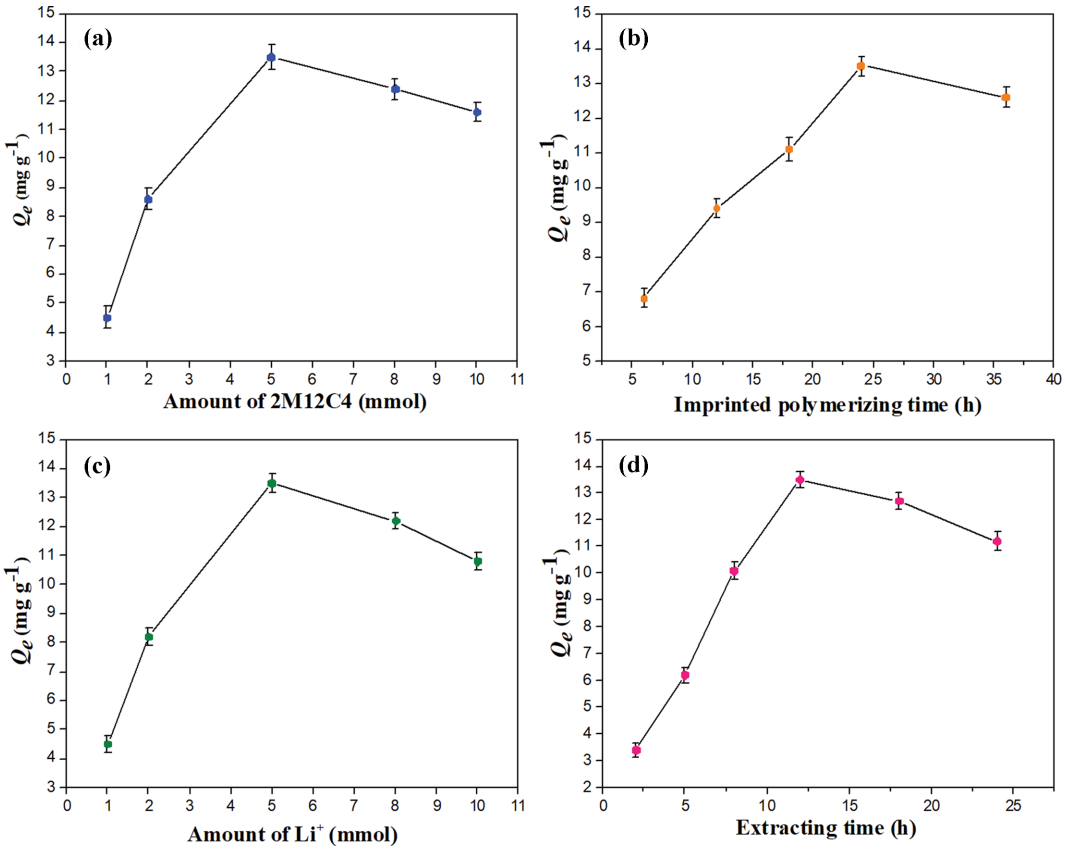


**Fig. 6. Effects of (a) the amount of 2M12C4, (b) imprinted polymerizing time, (c) the amount of $Li^+$ and (d) extracting time on the adsorption capacity of LiI-NcMs. Error bars are standard deviations from three experiments with independently prepared membranes.**

the contact angle of LiI-NcMs was 55.1°: this result demonstrates that the GR/$TiO_2$ nanocomposite has more outstanding species in the hydrophilicity. The phenomenon should be ascribed to GR/$TiO_2$ nanocomposite introducing more hydrophilic groups and leads to a rougher surface on the membrane. These meaningful results have provided the LiI-NcMs with better hydrophilicity.

**3. Optimization of Preparation Conditions**

To obtain the optimization preparation conditions, we studied the amount of 2M12C4, imprinted polymerizing time, the amount of $Li^+$ and extracting time on the adsorption capacity of LiI-NcMs.

As shown in Fig. 6(a), the adsorption capacity of LiI-NcMs increased with the increase of 2AM12C4, and reached the maximum at 5.0 mmol. Since then, LiI-NcMs adsorption began to decline. This may be because excessive 2AM12C4 hinders the binding of $Li^+$ to the imprinting site, resulting in the degradation of LiI-NcMs adsorption performance. Therefore, the optimal dosage of ligand 2AM12C4 is 5.0 mmol. And Fig. 6(b) shows that the adsorption capacity of LiI-NcMs increased with the increase of the imprinting polymerization time. Adsorption capacity reached the maximum adsorption capacity at 24 h and then gradually decreased, which may be because the imprinted polymer agglomerates on the membrane surface hindering the binding of $Li^+$ to the imprinted site. It can be observed from Fig. 6(c), when the amount of $Li^+$ is less than 5.0 mmol, the adsorption capacity of LiI-NcMs gradually increases, and reaches the maximum and then decreases. This may be due to the reaction of $Li^+$ in high concentration affecting the formation of recognition sites. As shown in Fig. 6(d), when the extracting time was 12 h, the LiI-NcMs had the best adsorption capacity.

**4. Evaluation of Membrane Performance**

4-1. Isothermal Adsorption and Kinetic Adsorption

In addition to the above characterizations, in order to more fully

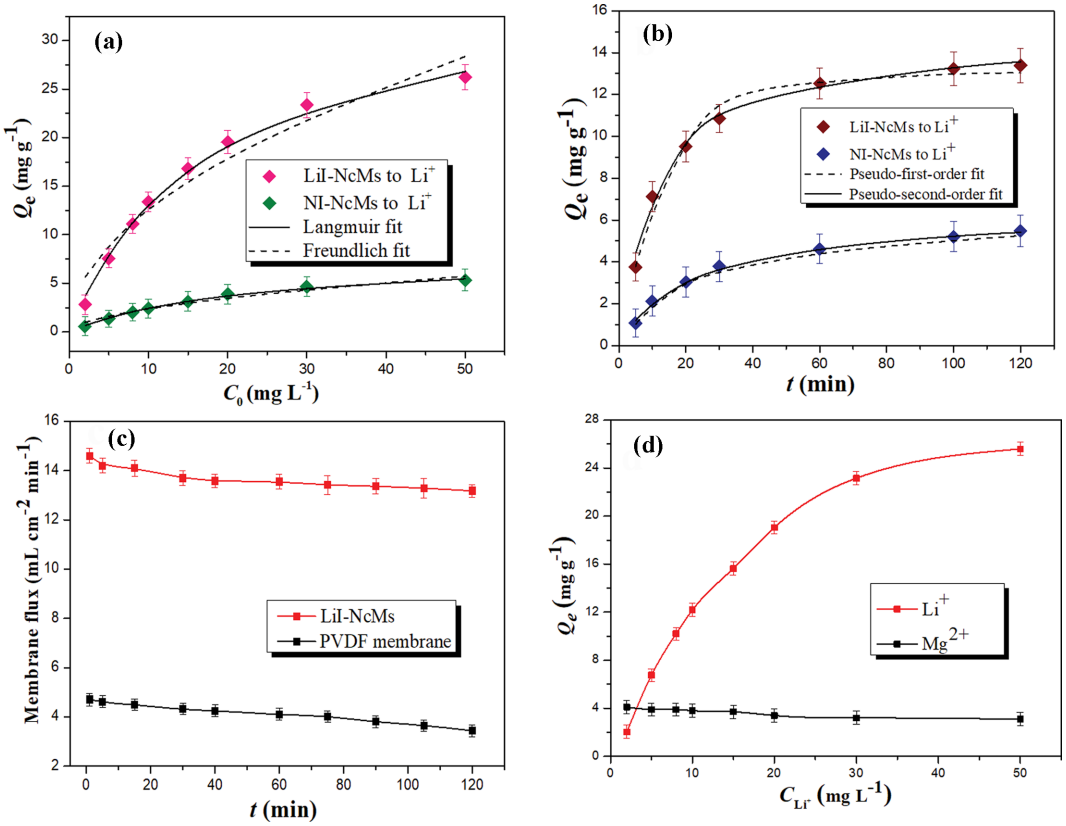


**Fig. 7. (a) Isothermal and (b) Kinetic adsorption of LiI-NcMs and NI-NcMs, (c) Membrane flux of PVDF membrane and LiI-NcMs, (d) Adsorption selectivity of LiI-NcMs. Error bars are standard deviations from three experiments with independently prepared membranes.**

**Table 1. Constants of isotherm onto LiI-NcMs and NI-NcMs**

| Membranes | Langmuir model | | | Freundlich model | | |
|---|---|---|---|---|---|---|
| | $K_L$ | $Q_{e,cal}$ | $R^2$ | $K_F$ | 1/n | $R^2$ |
| LiI-NcMs | 0.0564 | 36.336 | 0.9953 | 3.9757 | 0.5024 | 0.9434 |
| NI-NcMs | 0.0442 | 7.9386 | 0.9948 | 0.6739 | 0.5474 | 0.9545 |

explore the performance of prepared membranes, the static adsorption (concentration-depend rebinding) performance of LiI-NcMs and NI-NcMs was investigated. As to isothermal adsorption rebinding (Fig. 7(a)), with the increases initial concentration of $Li^+$, an upward tendency can be exhibited on equilibrium adsorption capacity of the LiI-NcMs and NI-NcMs. Meanwhile, compared with NI-NcMs, higher rebinding capacity of LiI-NcMs indicates a large amount of $Li^+$-imprinted sites onto LiI-NcMs, which could form interactions between $Li^+$ and $Li^+$-imprinted sites onto LiI-NcMs. In addition, the Langmuir and Freundlic isotherm adsorption models were used to fit the experimental data, as follows:

$$Q_e = \frac{K_L Q_m C_0}{1 + K_L C_0} \quad (7)$$

$$Q_e = K_F C_e^{1/n} \quad (8)$$

where $Q_e$ (mg $g^{-1}$) and $Q_m$ (mg $g^{-1}$) are adsorption capacity at equilibrium and saturated. $C_0$ (mg $L^{-1}$) and $C_e$ (mg $L^{-1}$) are concentrations before and after rebinding. n is measured surface unevenness. $K_L$ and $K_F$ are Langmuir and Freundlich constants.

The isothermal adsorption constants for LiI-NcMs and NI-NcMs are listed in Table 1. As shown in Fig. 7(a) and Table 1, the correlation coefficient ($R^2$) onto LiI-NcMs of the Langmuir model is 0.9953, and the linear regression value fits better with the Langmuir model than that of Freundlich model ($R^2$=0.9434) indicates that mono-layer recognition sites are distributed on surface of LiI-NcMs uniformly, and the rebinding is dependnt on one type of chemical groups [30-33].

Secondly, the kinetic adsorption (time-depended rebinding) of LiI-NcMs and NI-NcMs was studied. The kinetics of adsorption process controlled the adsorption time from 5.0 to 120 min. Adsorption capacity at different time is shown in Fig. 7(b). LiI-NcMs and NI-NcMs increase rapidly within 45 min and then nearly reach equilibrium at 60 min. It suggests the $Li^+$-imprinted sites for the rapid rebinding of $Li^+$ [16]. And the adsorption capacity of LiI-NcMs are always higher than NI-NcMs (consistent with isother-

**Table 2. Constants of kinetic onto LiI-NcMs and NI-NcMs**

| Membranes | Pseudo-first-order | | | Pseudo-second-order | | |
|---|---|---|---|---|---|---|
| | $Q_{e,cal}$ | $k_1$ ($min^{-1}$) | $R^2$ | $Q_{e,cal}$ | $k_2$ (g $mg^{-1}$ $min^{-1}$) | $R^2$ |
| LiI-NcMs | 13.0365 | 0.0685 | 0.9742 | 14.9044 | 0.0843 | 0.9931 |
| NI-NcMs | 5.2832 | 0.0434 | 0.9801 | 6.3883 | 0.0452 | 0.9668 |

mal adsorption), indicates that specific rebinding and non-specific rebinding on LiI-NcMs and NI-NcMs. To study the mechanism of kinetic adsorption, kinetic adsorption data of LiI-NcMs and NI-NcMs were fitted with pseudo-first-order and pseudo-second-order adsorption kinetics equation:

$$Q_t = Q_e e^{-k_i t} \quad (9)$$

$$Q_t = \frac{K_2 Q_e^2 t}{1 + K_2 Q_t t} \quad (10)$$

where $Q_e$ (mg $g^{-1}$) and $Q_t$ (mg $g^{-1}$) are adsorption capacity at equilibrium and time t (min), $K_1$ ($min^{-1}$) and $k_2$ (g $mg^{-1}$ $min^{-1}$) are pseudo-first-order and pseudo- second-order kinetic rate constants.

Table 2 lists the linear regression and adsorption rate constants for the pseudo-first-order and pseudo-second-order constants. From Fig. 7(b) and Table 2, it can be seen that the pseudo-second-order kinetic model ($R^2$=0.9931) of LiI-NcMs is better than the pseudo-first-order kinetic model ($R^2$=0.9742). At the same time, the pseudo-first-order kinetic model ($R^2$=0.9801) of NI-NcMs is better than the pseudo- second-order kinetic model ($R^2$=0.9668). It suggests that the chemical adsorption towards $Li^+$ is the main reason onto LiI-NcMs, as well as the physical adsorption is the main reason onto NI-NcMs [36]. This further proves the effectiveness of imprinted sites onto LiI-NcMs.

4-2. Membrane Flux

Fig. 7(c) shows the membrane flux of PVDF membrane and LiI-NcMs. The membrane flux of LiI-NcMs in the whole range of tested is always higher than PVDF membrane. Also, the flux of LiI-NcMs changes steadily with the increase of time. The reason should be attributed to the LiI-NcMs containing abundant oxygen-containing groups (hydroxyl, carboxyl, epoxide), which could effectively improve the hydrophilicity. Importantly, abundant $Li^+$-imprinted sites onto LiI-NcMs promoted mass transfer of $Li^+$.

4-3. Selective Adsorption

To further study the selective adsorption of LiI-NcMs, equilibrium adsorption capacity of LiI-NcMs in the mixed solution of $Mg^{2+}$ and $Li^+$ was explored. As shown in Fig. 7(d), even though the concentration of $Mg^{2+}$ is much higher than $Li^+$, LiI-NcMs also shows good adsorption capacity. This is due to the presence of $Li^+$-imprinted sites onto LiI-NcMs promoting the higher rebinding capacity of LiI-NcMs toward $Li^+$. It goes without saying that ion imprinting technology could improve the specific recognition and separation performance of membranes to target ion during the separation process.

4-4. Selective Permeation

The selective permeability of imprinted membrane material is an important indicator for testing overall performance. In this work, the selective permeation performance of LiI-NcMs and NI-NcMs

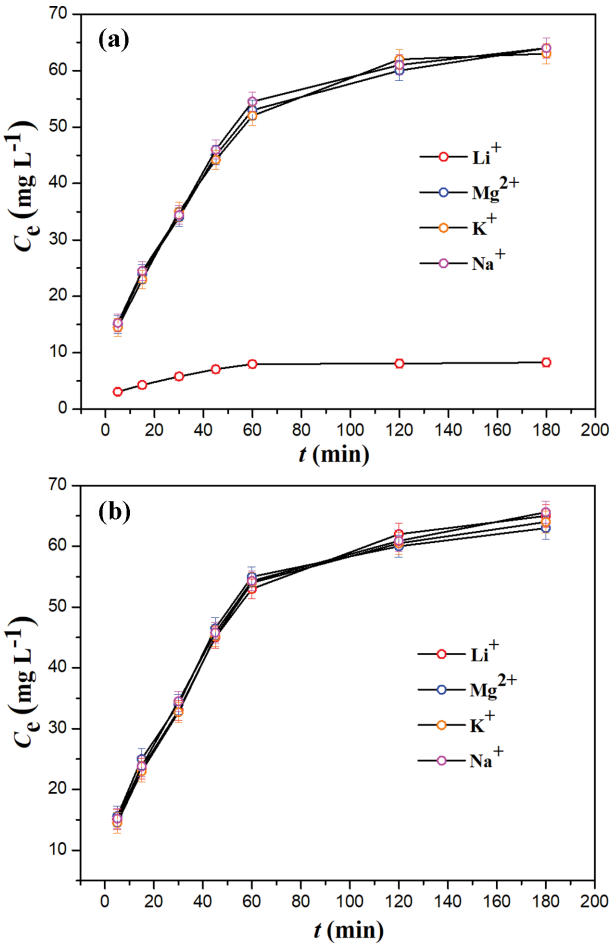


**Fig. 8. Permselectivity curves of (a) LiI-NcMs and (b) NI-NcMs. Error bars are standard deviations from three experiments with independently prepared membranes.**

was studied by competitive adsorption experiments (mixed aqueous solution of $Li^+$, $K^+$, $Na^+$ and $Mg^{2+}$ at a concentration of 100 mg $L^{-1}$). The time-dependent concentration curves and permeability of LiI-NcMs are shown in Fig. 8(a). LiI-NcMs exhibited a higher permeability toward competitive ion ($K^+$, $Na^+$ and $Mg^{2+}$) than that of target ion ($Li^+$). It should be ascribed to the $Li^+$-imprinted sites enhancing the effective binding between $Li^+$ and $Li^+$-imprinted sites during the permeation, which hinders the transmission of $Li^+$. It can be considered that the permeation process of $Li^+$, $K^+$, $Na^+$ and $Mg^{2+}$ through LiI-NcMs is a "delayed" osmotic mass transfer mechanism. As shown in Fig. 8(b), the permeability of NI-NcMs toward for $Li^+$, $K^+$, $Na^+$ and $Mg^{2+}$ is almost unanimity; this further proves the effectiveness of $Li^+$-imprinted sites onto LiI-

**Table 3. Permeation test results of LiI-NcMs and NI-NcMs**

| Membranes | Ions | $J_x$ (mg cm$^{-2}$ s$^{-1}$)*10$^{-5}$ | P (cm$^2$s$^{-1}$)*10$^{-5}$ | $\beta_{M/lithium}$ |
|---|---|---|---|---|
| LiI-NcMs | $Li^+$ | 6.09 | 0.39 | |
| | $Mg^{2+}$ | 23.65 | 3.35 | 8.58 |
| | $K^+$ | 22.74 | 3.21 | 8.23 |
| | $Na^+$ | 23.52 | 3.24 | 8.30 |
| NI-NcMs | $Li^+$ | 24.38 | 4.39 | |
| | $Mg^{2+}$ | 24.33 | 4.24 | 0.96 |
| | $K^+$ | 24.29 | 4.32 | 0.98 |
| | $Na^+$ | 24.42 | 4.43 | 1.01 |

**Table 4. Comparison of the adsorbent developed in this work with other reported materials**

| Absorbent | Sample | $Li^+$ concentration (mg L$^{-1}$) | Adsorption capacity (mg g$^{-1}$) | Refs. |
|---|---|---|---|---|
| HTO/PAN | $Li^+$ solution | 70 | 32 | 35 |
| HMO/AL | LiCl solution | 29.35 | 24 | 36 |
| HMO/PVDF | LiOH solution | 117.98 | 19.22 | 37 |
| PVA/HTO | LiCl/LiOH solution | 7 | 12 | 38 |
| $H_{1.6}Mn_{1.6}O_4$/PAN | LiCl/LiOH solution | 35 | 10.3 | 39 |
| LiI-NcMs | LiCl solution | 10 | 13.3 | This work |

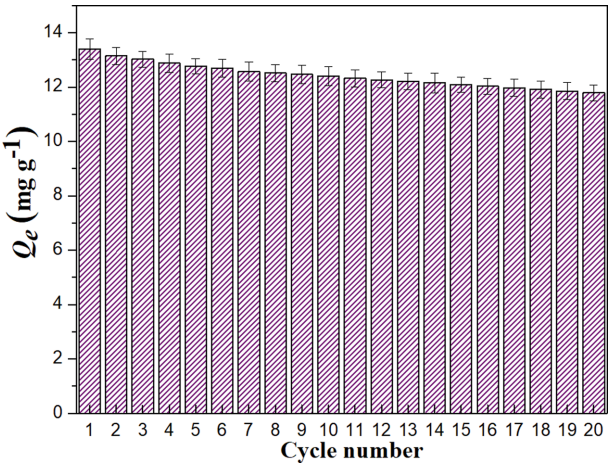


**Fig. 9. Stability performance on the rebinding capacity of the LiI-NcMs. Error bars are standard deviations from three experiments with independently prepared membranes.**

NcMs.

In addition, parameters of permeation onto LiI-NcMs and NI-NcMs are summarized in Table 3. The maximum permeability factor $\beta$ was 8.58, indicating that LiI-NcMs have excellent imprinting effect and better selectivity toward $Li^+$.

**5. Stability Performance**

For comprehensive evaluation of the stability performance, the adsorption/desorption cycle was repeated 20 times. 10 mg L$^{-1}$ $Li^+$ solution was used as the adsorption solution. After the adsorption reached equilibrium, the saturated LiI-NcMs were eluted with 0.5 mol/L HCl solution. Then the LiI-NcMs were further subjected to another adsorption/desorption cycle. It can be seen from Fig. 9, LiI-NcMs is able to maintain 88.1% of its initial rebinding capacity after 20 cycles, indicating that LiI-NcMs can be reused for many times without significant differences in adsorption capacity. The service life of the obtained membrane plays an important role in the evaluation of membrane performance.

**6. Comparison of the Adsorbent Developed in this Work with other Reported Materials**

As shown in Table 4 [34], although the adsorption capacity of some materials is more than LiI-NcMs, the concentration of $Li^+$ solutions is much higher than our study in this work. These results in Table 4 once again indicate that the LiI-NcMs developed in this work would play a positive role in promoting the development and applications of membranes in selectively separating $Li^+$ in water.

## CONCLUSION

An antifouling imprinted composite membrane for selective separation of Li ions has been developed. GO and $TiO_2$ nanocomposite material were employed for improved hydrophilicity and antifouling. The contact angle of LiI-NcMs was 55.1° and BSA adsorption capacity demonstrated a better antifouling property. LiI-NcMs also showed good adsorption capacity, indicating the presence of $Li^+$-imprinted sites could promote higher rebinding capacity of LiI-NcMs toward $Li^+$. This work opens new opportunities for designing and fabricating ion-imprinted nanocomposite membrane for selective separation of lithium ion.

## ACKNOWLEDGEMENT

This work was supported by the National Natural Science Foundation (No. 22004047), Project of Education Department of Jilin Province (JJKH20200427KJ), Projects of Jilin Province Development and Reform Commission (2021C036-7 and 2021C038-7), Project of Department of Science & Technology of Jilin Province

(20180623042TC).

## REFERENCES


1. J. Zhang, Y. Ai, J. Wu, D. Zhang, Y. Wang, Z. Feng, H. Sun, Q. Liang, T. Sun and Y. Yang, *Adv. Funct. Mater.*, **30**, 1904645 (2020).
2. Y. Wang, R. Guo, W. Liu, L. Zhu, W. Huang, W. Wang and H. Zheng, *J. Power Sources*, **444**, 227260 (2019).
3. B. Shanmugam, P. Ignacimuthu and S. Nallani, *Appl. Surf. Sci.*, **498**, 143792 (2019).
4. Y. Yang, P. Peng, Q. Yang, D. Wang and J. Dong, *Appl. Surf. Sci.*, **530**, 147163 (2020).
5. J. Lu, Y. Qin, Q. Zhang, C. Yu, Y. Wu, Y. Yan, H. Fan, M. Meng and C. Li, *Chem. Eng. J.*, **360**, 483 (2019).
6. N. Amaly, Y. Ma, A. El-Moghazy and G. Sun, *Sep. Purif. Technol.*, **250**, 117086 (2020).
7. J. Lu, Y. Qin, C. Li, Y. Wu, M. Meng, Z. Dong, C. Sun, M. Chen and Y. Yan, *Chem. Eng. J.*, **405**, 126716 (2021).
8. X. Ying, X. Zhu, A. Kang and X. Li, *Talanta*, **204**, 647 (2019).
9. M. Bengamra, N. Grayaa-Jaoued, A. Khlifi-Riani, M. Chehimi and R. Kalfat, *Silicon*, **11**, 2267 (2019).
10. Y. Liu, Z. Yan, R. Chen, Y. Yu, X. Chen, X. Zheng and X. Huang, *J. Hazard. Mater.*, **377**, 259 (2019).
11. J. Guo, D. Yan, F. L. Lam, B. J. Deka, X. Lv, Y. H. Ng and A. K. An, *Chem. Eng. J.*, **378**, 122137 (2019).
12. Y. S. Khoo, W. J. Lau, Y. Liang, M. Karaman, M. Gürsoy and A. F. Ismail, *Sep. Purif. Technol.*, **250**, 116976 (2020).
13. J. Lu, Y. Wu, X. Lin, J. Gao, H. Dong, L. Chen, Y. Qin, L. Wang and Y. Yan, *J. Hazard. Mater.*, **353**, 244 (2018).
14. N. Li, J. Zhang, Y. Tian, J. Zhao, J. Zhang and W. Zuo, *Chem. Eng. J.*, **304**, 165 (2016).
15. F. Gao, J. Wang, H. Zhang, Y. Zhang and M. Hang, *J. Membr. Sci.*, **519**, 22 (2016).
16. J. Lu, Y. Qin, Y. Wu, M. Chen, C. Sun, Z. Han, Y. Yan, C. Li and Y. Yan, *Chem. Eng. J.*, **417**, 128085 (2021).
17. J. Zhu, J. Hou, Y. Zhang, M. Tian, T. He, J. Liu and V. Chen, *J. Membr. Sci.*, **550**, 173 (2018).
18. M. Cruz, G. Ruano, M. Wolf, D. Hecker, E. Vidaurre, R. Schmittgens and V. Rajal, *Chem. Eng. Res. Des.*, **94**, 524 (2015).
19. H. Palza, *Int. J. Mol. Sci.*, **16**, 2099 (2015).
20. H. Hegab and L. Zou, *J. Membr. Sci.*, **484**, 95 (2015).
21. S. Zheng, Q. Tu, J. Urban, S. Li and B. Mi, *ACS Nano*, **11**, 6440 (2017).
22. N. Padmavathy, S. Behera, S. Pathan, L. Ghosh and S. Bose, *ACS Appl. Mater. Inter.*, **11**, 7566 (2019).
23. N. Haghighat, V. Vatanpour, M. Sheydaei and Z. Nikjavanb, *Sep. Purif. Technol.*, **237**, 116374 (2020).
24. X. Zhao, Y. Lan, K. Yang, R. Wang, L. Cheng and C. Gao, *Appl. Surf. Sci.*, **525**, 146564 (2020).
25. Y. Xu, H. Bai, G. Lu, C. Li and G. Shi, *J. Am. Chem. Soc.*, **130**, 5856 (2008).
26. C. Nethravathi and M. Rajamathi, *Carbon*, **46**, 1994 (2008).
27. D. Sun, M. Meng, Y. Qiao, Y. Zhao, Y. Yan and C. Li, *Sep. Purif. Technol.*, **194**, 64 (2018).
28. Y. Xu, Y. Zhuang and X. Fu, *J. Phys. Chem. C*, **114**, 2669 (2010).
29. D. Sun, M. Meng, Y. Lu, B. Hu, Y. Yan and C. Li, *New J. Chem.*, **42**, 4432 (2018).
30. J. Fan, L. Li, Z. Tian, C. Xie, F. Song, X. Zhang and J. Zhu, *J. Membr. Sci.*, **467**, 13 (2014).
31. E. Turiel, C. Perez-Conde and A. Martin-Esteban, *Analyst*, **128**, 137 (2003).
32. J. Lu, Y. Qin, Y. Wu, M. Meng, Z. Dong, C. Yu, Y. Yan and C. Li, *J. Membr. Sci.*, **601**, 117917 (2020).
33. S. Liu, J. Pan, H. Zhu, G. Pan, F. Qiu, M. Meng, J. Yao and D. Yuan, *Chem. Eng. J.*, **290**, 220 (2016).
34. H. Lin, X. Yu, M. Li, J. Duo, Y. Guo and T. Deng, *ACS Appl. Mater. Inter.*, **11**, 26364 (2019).
35. C. Lawagon, G. Nisola, R. Cuevas, H. Kim, S. Lee and W. Chung, *J. Ind. Eng. Chem.*, **70**, 124 (2019).
36. P. Koilraj, S. Smith, Q. Yu, S. Ulrich and K. Sasaki, *Powder Technol.*, **301**, 1201 (2016).
37. S. Zandvakili and M. Ranjbar, *Miner. Process. Extr. Metall.*, **127**, 176 (2018).
38. L. Limjuco, G. Nisola, C. Lawagon, S. Lee, J. Seo, H. Kim and W. Chung, *Colloids Surf. A*, **504**, 267 (2016).
39. M. Park, G. Nisola, A. Beltran, R. Torrejos, J. Seo, S. Lee, H. Kim and W. Chung, *Chem. Eng. J.*, **254**, 73 (2014).